Xia *et al. Natural Products and Bioprospecting* (2025) 15:65
https://doi.org/10.1007/s13659-025-00548-1

Natural Products and Bioprospecting

ORIGINAL ARTICLE Open Access

Strophioglandins A–C, highly rearranged norditerpenoids with an unusual tricyclo[6.4.1.0^{4,13}]tridecane core from *Strophioblachia glandulosa* var. *cordifolia*

Jian-Kai Xia[1], Lei-Ming Wu[1], Wei-Ye Wu[1], Dong Huang[1], Fang-Yu Yuan[1], Lei Li[1], Shu-Qi Wu[1], Yan-Jiang Zhang[1], Tao Yuan[2], Xin Chen[3], Gui-Hua Tang[1], Jia-Luo Huang[1*] and Sheng Yin[1*]

Abstract

Strophioglandins A–C (**1**–**3**), three highly rearranged norditerpenoids featuring an unusual tricyclo[6.4.1.0^{4,13}]tridecane core, were isolated from *Strophioblachia glandulosa* var. *cordifolia*. Integrated spectroscopic analyses, X-ray crystallography, and ECD calculations synergistically determined their molecular architectures. Remarkably, all compounds manifested potent anti-inflammatory effects in LPS-activated RAW264.7 cells with IC_{50} values ranging from 7.83 ± 1.11 to 15.09 ± 1.21 μM. Mechanism study revealed that strophioglandin A (**1**), the most potent compound, could suppress the expression of multiple inflammatory factors by inhibiting the P38 and Erk1/2 MAPK signaling pathways.

Keywords *Strophioblachia glandulosa* var. *cordifolia*, Rearranged norditerpenoids, Anti-inflammatory effects, MAPK signaling pathways

*Correspondence:
Jia-Luo Huang
huangjluo3@mail.sysu.edu.cn
Sheng Yin
yinsh2@mail.sysu.edu.cn
Full list of author information is available at the end of the article

Graphical Abstract

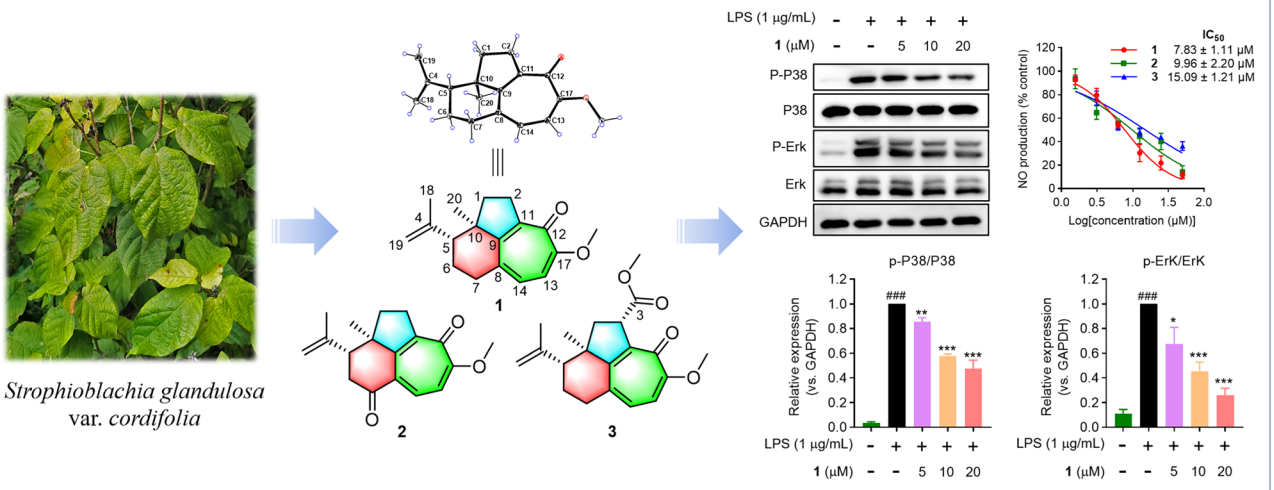

1 Introduction

Euphorbiaceae plants are well known for producing structurally intricate macrocyclic and polycyclic diterpenoids with a broad range of bioactivities [1–6]. The pharmacological and chemical significance of these diterpenoids drives sustained research interest, because they not only serve as potential leads in drug discovery but also pose formidable synthetic challenges that inspire novel methodology design in organic chemistry. For instance, ingenol mebutate, an ingenane ester isolated from *Euphorbia peplus* L., received Food and Drug Administration (FDA) approval in 2012 as a treatment for actinic keratosis [7]. Its precursor, (+)-ingenol, featuring a 5/7/7/3 tetracyclic architecture, has been elaborately synthesized in only 14 steps using a two-phase strategy [8, 9]. (−)-Pepluanol B, a potassium channel inhibitor with an unusual 5/5/8/3 ring system, has been totally synthesized via an unprecedented bromo-epoxidation maneuver [10].

Strophioblachia glandulosa var. *cordifolia* is a shrub distributed in southern Yunnan, China. Its chemical constituents have not been investigated to date. Previous phytochemical investigations on other species within *Strophioblachia* (Euphorbiaceae) have identified a series of structurally unique diterpenoids, some of which exhibited cytotoxic, anti-inflammatory, proliferation inhibition, neuroprotective, and anti-myocardial hypertrophy activities [11–14].

As part of our ongoing quest for bioactive natural products [15–18], three highly rearranged norditerpenoids, strophioglandins A–C (**1**–**3**), featuring an unusual tricyclo[6.4.1.$0^{4,13}$]tridecane core (Fig. 1), were isolated from the twigs and leaves of *S. glandulosa* var. *cordifolia*. Their structures, including the absolute configurations, were identified by HRESIMS, spectroscopic methods, X-ray crystallography, and ECD calculations. Herein, we detail their structural characterization, putative biosynthetic pathways, anti-inflammatory effects, and the underlying mechanism.

2 Results and discussion

Strophioglandin A (**1**) was obtained as colorless needle crystals with a molecular formula $C_{18}H_{22}O_2$ as determined by the HRESIMS ion at *m*/*z* 293.1518 $[M+Na]^+$ (calcd. for $C_{18}H_{22}O_2Na^+$, 293.1512), indicating eight indices of hydrogen deficiency (IHDs). The ^{1}H NMR data (Table 1) displayed signals for two methyl groups [(δ_H 1.02 (s) and 1.84 (s)], a methoxy [δ_H 3.89 (s)], two *cis*-olefinic protons [δ_H 6.65 (1H, d, J = 10.3 Hz) and 6.87 (1H, d, J = 10.3 Hz)], two terminal double bond protons [δ_H 4.77 (s) and 4.95 (s)], and a series of aliphatic multiplets.

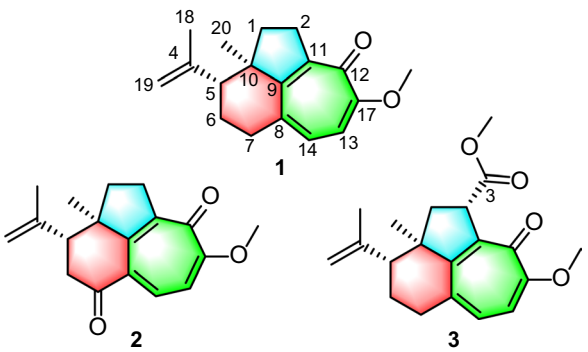

Fig. 1 The structures of compounds **1**–**3**

Table 1 ^{1}H (400 MHz) and ^{13}C (100 MHz) NMR data of **1–3** in $CDCl_3$ (δ in ppm, *J* in Hz)

No	1		2		3	
	δ_H, multi. (*J*)	δ_C, type	δ_H, multi. (*J*)	δ_C, type	δ_H, multi. (*J*)	δ_C, type
1*α*	1.87, m	38.1, CH_2	1.95, m	37.4, CH_2	2.07, m	41.4, CH_2
1*β*	1.89, m		1.98, m		2.37, m	
2	*α*, 2.95, overlapped *β*, 3.16, m	32.0, CH_2	*α*, 3.06, m *β*, 3.24, m	32.8, CH_2	4.32, d (11.0)	49.5, CH
3						174.7, C
4		146.3, C		143.6, C		145.7, C
5	2.29, dd (12.9, 3.9)	50.9, CH	2.83, m	49.3, CH	2.30, dd (12.6, 4.7)	51.1, CH
6*α*	2.06, m	24.6, CH_2	2.91, m	39.4, CH	2.04, m	24.4, CH_2
6*β*	1.80, m		2.62, dd (17.4, 3.0)		1.82, m	
7	*α*, 2.98, overlapped; *β*, 2.79, m	32.1, CH_2		198.3, C	*α*, 3.01, m *β*, 2.79, m	31.4, CH_2
8		136.5, C		129.2, C		136.1, C
9		157.1, C		157.3, C		157.8, C
10		52.2, C		52.2, C		52.6, C
11		148.7, C		147.7, C		144.3, C
12		177.1, C		176.9, C		176.8, C
13	6.65, d (10.3)	112.2, CH	6.86, d (10.7)	110.5, CH	6.64, d (10.3)	112.1, CH
14	6.87, d (10.3)	130.8, CH	8.09, d (10.7)	135.8, CH	6.93, d (10.3)	131.8, CH
17		162.5, C		166.9, C		163.1, C
18	1.84, s	24.4, CH_3	1.88, s	24.2, CH_3	1.84, s	23.9, CH_3
19a	4.95, s	113.2, CH_2	5.07, s	114.6, CH_2	4.95, s	113.9, CH_2
19b	4.77, s		4.86, s		4.80, s	
20	1.02, s	19.6, CH_3	1.18, s	18.6, CH_3	1.15, s	21.3, CH_3
3-OMe					3.69, s	52.2, CH_3
17-OMe	3.89, s	56.1, CH_3	4.03, s	57.0, CH_3	3.89, s	56.1, CH_3

The 1D NMR data (Table 1) of **1** showed 18 carbon resonances ascribed to a ketone carbonyl (δ_C 177.1), four double bonds (δ_C 162.5, 157.1, 148.7, 146.3, 136.5, 130.8, 113.2, 112.2), a methoxy group (δ_C 56.1), two methyls, four sp^3 methylenes, an sp^3 methine, and a quaternary carbon. As five of the eight IHDs were consumed by four double bonds and a ketone carbonyl, the remaining three IHDs were indicative of a tricyclic ring system.

The planar structure of **1** was determined through comprehensive analysis of its 2D NMR data, including HSQC, $^{1}H–^{1}H$ COSY, and HMBC spectra. The key HMBC correlations from Me-20 to C-1/C-9/C-10 and from H_2-2 to C-9/C-10/C-11, along with the $^{1}H–^{1}H$ COSY correlation of H_2-1/H_2-2 (Fig. 2), constructed a fragment of five-membered ring A with Me-20 located at C-10. Additionally,$^{1}H–^{1}H$ COSY spectrum of H-5/H_2-6/H_2-7, together with the HMBC cross-peaks from Me-20 to C-5/C-9/C-10 and from H_2-7 to C-5/C-8/C-9 instructively established a six-membered ring B, which was fused with ring A by sharing C-9 and C-10. A typical isopropenyl group was positioned at C-5 in ring B as elucidated by the HMBC correlations from Me-18 to

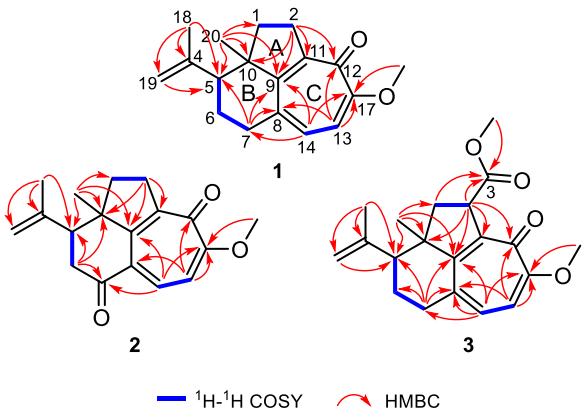

Fig. 2 $^{1}H–^{1}H$ COSY and key HMBC correlations of **1–3**

C-5 and the terminal double bond (δ_C 113.2 and 146.3), as well as from H_2-19 to C-5. The $^{1}H–^{1}H$ COSY correlation of H-13/H-14 and the HMBC correlations from H_2-2 to C-9/C-11/C-12, from H-13 to C-8/C-12/C-17, from H-14 to C-7/C-9/C-17, and from OMe-17 to C-17, led to the confirmation of a tropolone nucleus (ring C) with a

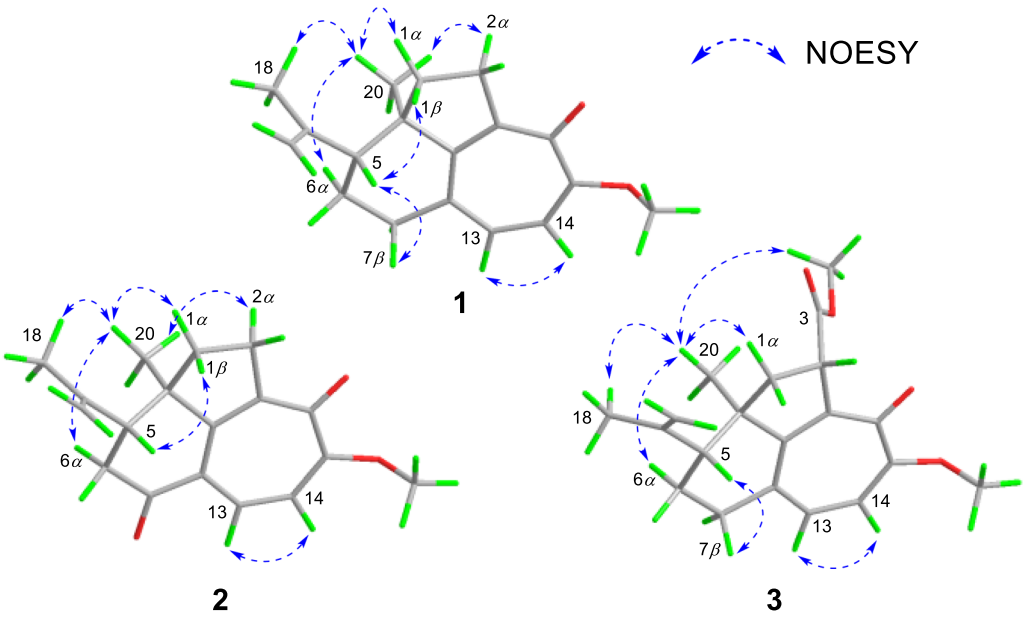

Fig. 3 Key NOESY correlations of **1**–**3**

ketone carbonyl (δ_C 177.1) and a methoxy group (δ_C 56.1 and δ_H 3.89) assigned at C-12 and C-17, respectively. Hence, the planar structure of **1** was established (Fig. 2), featuring a rare tricyclo[6.4.1.$0^{4,13}$]tridecane core.

NOESY experiment enabled determination of the relative configuration of compound **1** (Fig. 3). The NOESY spectrum revealed a cross-peak between Me-18 and Me-20, indicating spatial proximity between the isopropenyl group and Me-20. These groups were thus assigned as co-facial and α-oriented. Therefore, the relative stereochemistry 5*R**,10*R** was assigned to **1**. The 5*R*,10*R* absolute configuration of **1** was establishedby X-ray crystallography [Flack parameter: −0.06(10); CCDC number: 2422939] (Fig. 4).

The HRESIMS data (*m*/*z* 307.1302 $[M+Na]^+$, calcd. for $C_{18}H_{20}O_3Na^+$, 307.1305) established the molecular formula of strophioglandin B (**2**) as $C_{18}H_{20}O_3$, implying nine IHDs. NMR data comparison (Table 1) indicated that **2** shares a core structure with **1**, differing only by oxidation of the C-7 methylene (CH_2-7) in **1** to the carbonyl group in **2**, which was identified by signals from H_2-6 to C-5/C-7(δ_C 198.3)/C-10 and from H-14 to C-7 in its HMBC spectrum, as well as the cross-peak (H-5 and H_2-6) in the $^1H-^1H$ COSY

experiment (Fig. 2). Spatial proximity between Me-20 and the isopropenyl moiety was confirmed by NOESY (Fig. 3), establishing their α-configurational assignment. Biosynthetic considerations suggest congruent absolute configuration between **1** and **2**, which was further supported by the comparable ECD curves of **2** and (5*R*,10*R*)-**2a** (Fig. 5).

The ion peak at *m*/*z* 329.1751 ($[M+H]^+$, calcd. for $C_{20}H_{25}O_4^+$, 329.1747) in the HRESIMS spectrum assigned a molecular formula $C_{20}H_{24}O_4$ to strophioglandin C (**3**). Comprehensive NMR data analysis established **3** as a structural analogue of **1**, differing only by the replacement of one hydrogen at CH_2-2 with a methoxycarbonyl group, which was substantiated by correlations from H-2 to C-3/C-9/C-10/C-11/C-12 and from H_3-OMe-3 to C-3 (δ_C 174.7) in the HMBC experiment, coupled with the $^1H-^1H$ COSY cross-peak of H_2-1/H-2 (Fig. 2). Therefore, we established the planar constitution of **3** as shown in Fig. 2. The NOESY spectrum showed key cross-peaks of Me-18/Me-20 and OMe-3/Me-20, implying they possessed spatial proximity and were arbitrarily defined as α-orientated. The relative stereochemistry 2*S**,5*R**,10*R** was thus ascertained for **3**. The absolute configuration 2*S*,5*R*,10*R* was further given for

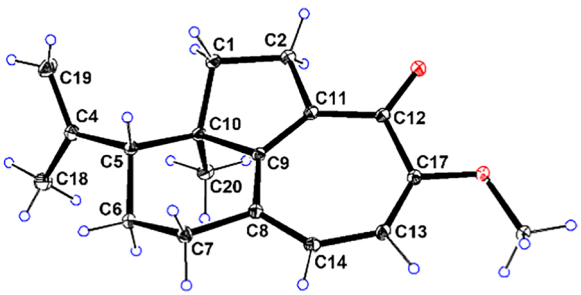

Fig. 4 X-ray ORTEP diagram of **1**

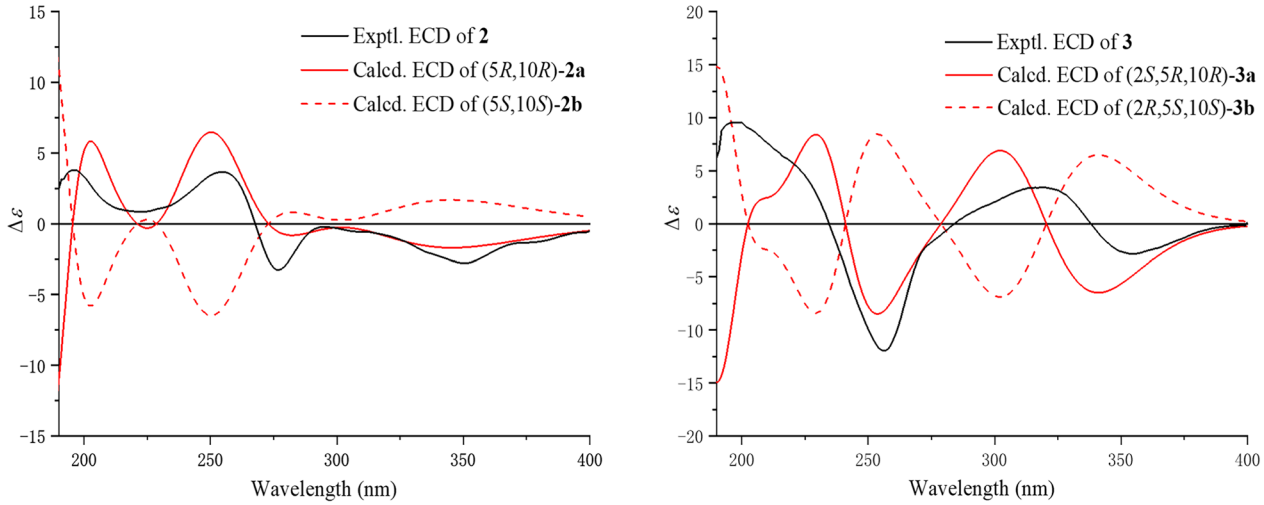

Fig. 5 Experimental and calculated ECD curves of **2** and **3**

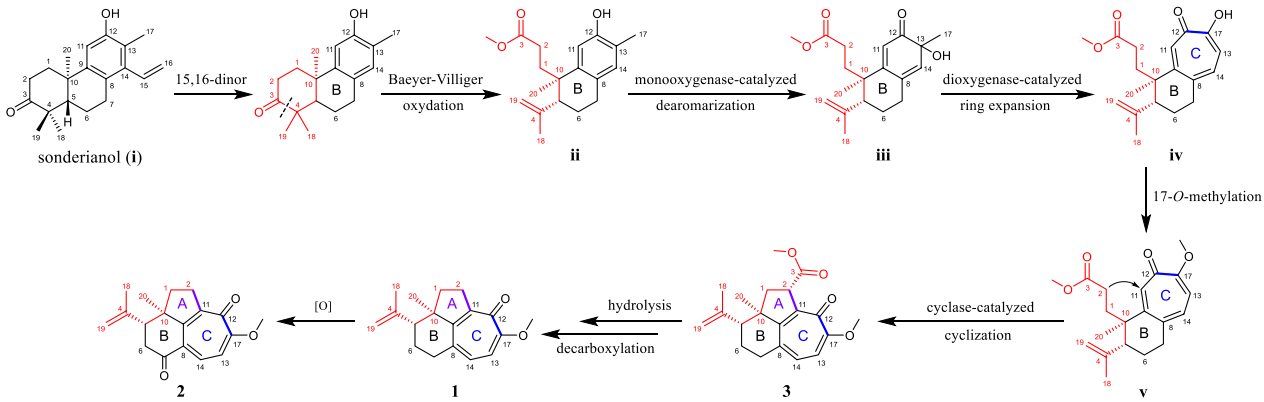

Scheme 1 Proposed biosynthetic pathways for **1**–**3**

3 as supported by the comparable ECD curves of **3** and (2*S*,5*R*,10*R*)-**3a** (Fig. 5).

We propose putative biosynthetic pathways for **1**–**3** to get a better understanding of their structures (Scheme 1). First, sonderianol (**i**), a cleistanthane diterpenoid isolated from the same genus, was considered as a biosynthetic precursor, which may undergo carbon degradation and Baeyer–Villiger oxidation to form a 3,4-*seco* intermediate (**ii**). **ii** was then dearomatized via hydroxylation at C-13 catalyzed by monooxygenase [19]. A key tropolone nucleus (ring C) in **iv** was generated via dioxygenase-catalyzed ring expansion of **iii** [19]. The 17-*O*-methylation of **iv** afforded **v**, followed by the cyclase-catalyzed cyclization (attack from C-2 to C-11) to form compound **3** [20, 21]. Subsequently, **3** underwent hydrolysis and decarboxylation to afford **1**, which could further produce **2** by the oxidation at C-7.

The suppression of lipopolysaccharide (LPS)-induced nitric oxide (NO) production in Raw264.7 macrophages by all isolates was measured to evaluate their anti-inflammatory effects. Preliminary screening suggested that **1**–**3** had potent inhibitory activities (IC_{50}s = 7.83–15.09 μM) (Fig. 6A) compared with the recognized NO inhibitor, quercetin (IC_{50} = 14.55 μM) [22, 23]. Meanwhile, the non-cytotoxicities of **1**–**3** to Raw264.7 cells at 50 μM indicated that their inhibitory activities did not result from cytotoxic effect. (Fig. 6B). Pro-inflammatory mediators generated by macrophages are potential biomarkers in the process of inflammation, such as PGE2, NO, IL-6, and TNF-*α* [22]. Subsequently, the effects of the most potent compound, strophioglandin A (**1**), on mRNA and the proteins levels were investigated in Raw264.7 macrophages. Pretreatment of **1** could dose-responsively suppress the LPS-triggered iNOS/COX-2 overexpression (Fig. 6C). Additionally, dose-responsive suppression of iNOS/IL-6/TNF-*α* transcription by **1** at concentrations of 5, 10, and 20 μM was evidenced as shown in Fig. 6D. The experiments mentioned above demonstrated that **1** could

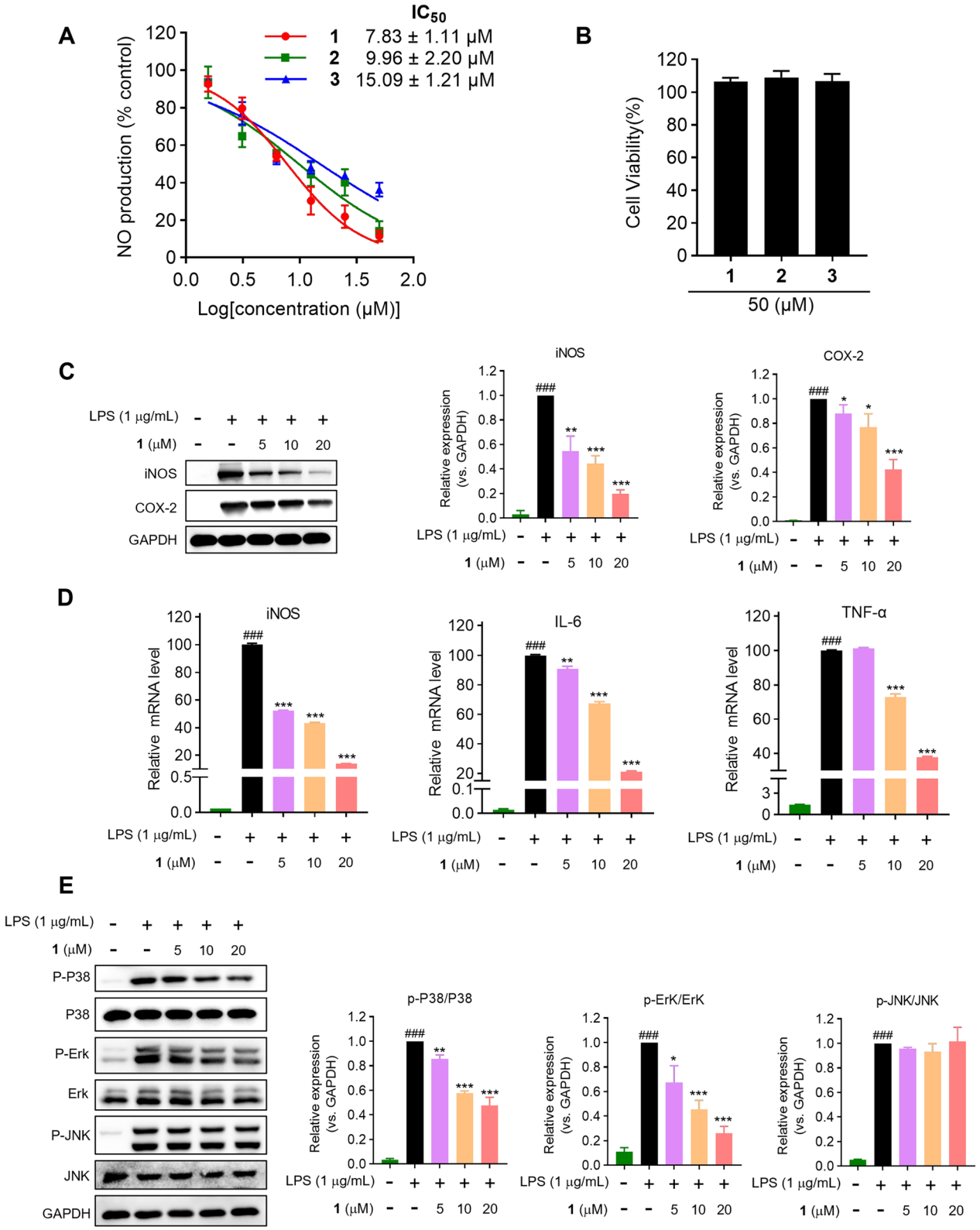

Fig. 6 The anti-inflammatory effects of **1**–**3** in Raw264.7 cells. **A** Inhibitory effects of **1**–**3** on NO production. **B** The cytotoxicities of **1**–**3** measured by CCK-8 reagent. **C** Inhibitory effects of **1** on the expression of COX-2 and iNOS. **D** Inhibitory effects of **1** on mRNA levels by qRT-PCR analysis. **E** Immunoblot analysis of MAPK pathway proteins. The data were presented as the mean ± SD of at least three experiments. $^{###}P < 0.001$ *vs* control group; $^{*}P < 0.05$, $^{**}P < 0.01$, $^{***}P < 0.001$ *vs* LPS group

suppress the up-regulation of multiple inflammation-associated factors in LPS-triggered murine macrophages.

Mitogen activated protein kinases (MAPK) signaling transduced by Toll-like receptors (TLRs) governs inflammatory effector expression in LPS-activated macrophages [24]. Consequently, Western blotting was employed to determine whether **1** could suppress the activated MAPK signaling pathways, specifically P38, Erk1/2, and JNK. As demonstrated in Fig. 6E, the pretreatment of **1** could dose-responsively constrain the P38 and Erk1/2 phosphorylation after brief (10 min) LPS-stimulation, while being ineffective against the JNK phosphorylation. These experiments verified that compound **1** could selectively curtail P38 and Erk1/2 phosphorylation (JNK unaffected), attenuating key inflammatory effectors expression.

3 Experimental section

3.1 General experimental procedures

These are provided in the Supporting Information.

3.2 Plant material

We collected the twigs and leaves of *S. glandulosa* var. *cordifolia* from Yuanjiang County, Yunnan Province in August 2023. The plant was then identified by G.-H. Tang.

3.3 Extraction and isolation

Twigs and leaves of *S. glandulosa* var. *cordifolia* (14.5 kg, dry weight) were powdered and extracted, under ambient conditions, thrice with 95% ethanol (3×75 L), generating a crude extract Weighing 1.2 kg. An aqueous suspension of the crude extract was subjected to liquid–liquid partition against petroleum ether (PE), followed by ethyl acetate (EtOAc), and then *n*-butanol (*n*-BuOH). Fractionation of the EtOAc extract (280.0 g) on D101 macroporous resin chromatographic column (CC), using MeOH/H_2O (3:1 → 1:0, *v*/*v*), yielded two fractions (Fr. I and Fr. II). Fr. I (86.2 g) was subjected to a silica gel column using CH_2Cl_2/MeOH (1:0 → 0:1, *v*/*v*), yielding eight subfractions (Fr. IA–Fr. IH). Among these, subfraction Fr. IB (10.0 g) was further subjected to silica gel chromatography using a PE/EtOAc gradient (8:1 → 0:1, *v*/*v*), affording nine fractions (Fr. IB_1–Fr. IB_9). Fr. IB_8 (1.5 g) was further subjected to Sephadex LH-20 CC (MeOH), affording compounds **1** (20.5 mg, t_R = 18.2 min), **2** (3.2 mg, t_R = 19.3 min), and **3** (16.8 mg, t_R = 15.6 min) followed by semi-preparative HPLC refinement (MeCN/H_2O, 48:52, *v*/*v*; 3.0 mL/min).

3.4 Spectroscopic data of the compounds

3.4.1 Strophioglandin A (1)

Colorless crystal; $[\alpha]_D^{20}$−160 (*c* 0.1, MeCN); UV (MeCN) λ_{max} (log ε) 253 (4.42), 333 (3.90) nm; ECD (*c* 7.40×10^{-4}, MeCN) λ_{max} ($\Delta\varepsilon$) 232 (+1.70), 354 (−3.07) nm; IR (neat) ν_{max} 2948, 2857, 1584, 1559, 1455, 1256, 1190, 1060, 1018, 890 cm^{-1}; ^1H and ^{13}C NMR data, see Table 1; HRESIMS *m*/*z* 293.1518 $[M+Na]^+$ (calcd. for $C_{18}H_{22}O_2Na^+$, 293.1512).

3.4.2 Strophioglandin B (2)

Yellowish oil; $[\alpha]_D^{20}$−103 (*c* 0.1, MeCN); UV (MeCN) λ_{max} (log ε) 240 (4.16), 269 (4.31), 355 (3.89) nm; ECD (*c* 3.52×10^{-4}, MeCN) λ_{max} ($\Delta\varepsilon$) 196 (+3.80), 255 (+3.67), 277 (−3.26), 350 (−2.78) nm; IR (neat) ν_{max} 2960, 2925, 2853, 1683, 1585, 1456, 1261, 1187, 1055, 1007, 896 cm^{-1}; ^1H and ^{13}C NMR data, see Table 1; HRESIMS *m*/*z* 307.1302 $[M+Na]^+$ (calcd. for $C_{18}H_{20}O_3Na^+$, 307.1305).

3.4.3 Strophioglandin C (3)

Yellowish oil; $[\alpha]_D^{20}$−55 (*c* 0.1, MeCN); UV (MeCN) λ_{max} (log ε) 251 (4.45), 330 (4.00) nm; ECD (*c* 3.05×10^{-4}, MeCN) λ_{max} ($\Delta\varepsilon$) 256 (−11.97), 319 (+3.43) nm; IR (neat) ν_{max} 2948, 1732, 1568, 1454, 1343, 1259, 1180, 1073, 1003, 894, 845 cm^{-1}; ^1H and ^{13}C NMR data, see Table 1; HRESIMS *m*/*z* 329.1751 $[M+H]^+$ (calcd. for $C_{20}H_{25}O_4^+$, 329.1747).

3.5 Crystallographic data for 1

$C_{18}H_{22}O_2$ (*M* = 270.35 g/mol): orthorhombic, space group *P* 2_1 2_1 2_1 (no. 19), *a* = 6.19478(9) Å, *b* = 6.86349(9) Å, *c* = 34.2241(4) Å, α = 90°, β = 90°, γ = 90°, *V* = 1455.14(3) $Å^3$, *Z* = 4, *T* = 100 K, μ (Cu Kα) = 0.616 mm^{-1}, D_{calc} = 1.234 g/cm^{-3}, 14 428 reflections measured (5.164° ≤ 2θ ≤ 157.466°), 3052 unique (R_{int} = 0.0449, R_{sigma} = 0.0436), which were used in all calculations. The final R_1 was 0.0436 ($I > 2\sigma(I)$) and wR_2 was 0.1176 (all data). Flack parameter:−0.06(10). CCDC number: 2422939.

3.6 ECD calculations

These are provided in the Supporting Information for **2** and **3**.

3.7 Cell culture

Cell culture was performed according to the established protocol [25].

3.8 Cytotoxicity assay

Raw264.7 cells (5×10^4 cells/well), prior to compounds treatment for 24 h, were allowed to adhere in 96-well plates. Following 24 h incubation at 37 °C, cell viability was assessed by using CCK-8 reagent (Dojindo, Japan) with 10 μL reagent added per well. Absorbance was finally recorded by means of a multifunction microplate reader at 450 nm.

3.9 Analysis of NO production

Following a 24-h incubation period after plating Raw264.7 macrophages (5×10^4 cells/well) in 96-well plates, compounds were added at increasing concentrations (5, 10, and 20 μM) and incubated, with or without LPS (1 μg/mL), for 24 h in media. NO concentration in the culture medium was quantified using a Griess reagent kit, following the manufacturer's protocol. For the assay, 50 μL of Griess reagent was mixed with an equal volume of cell culture supernatant. With quercetin serving as the positive control, the absorbance at 540 nm, by means of a multifunction microplate reader, was measured.

3.10 qRT-PCR analysis

This was performed according to the established protocol [25].

3.11 Western blotting analysis

This was performed according to the established protocol [25].

3.12 Statistical analysis

Statistical analysis followed the approach of reference [25].

4 Conclusion

In summary, three highly rearranged cleistanthane norditerpenoids (**1**–**3**) featuring an unusual tricyclo[6.4.1.$0^{4,13}$]tridecane carbon core, were isolated from *S. glandulosa* var. *cordifolia*. Compounds **1** and **2** are the first reported trinorditerpenoids with a highly fused 5/7/6-tricyclic skeleton. Notably, bioactivity evaluation demonstrated that all isolates exhibited remarkable anti-inflammatory effects. Strophioglandin A (**1**), the most potent compound, attenuated LPS-induced secretion of key pro-inflammatory cytokines (iNOS, IL-6, and TNF-α) in murine macrophages via blockade of MAPK signaling (P38 and Erk1/2 phosphorylation). This study deepens the chemical investigation of the genus *Strophioblachia*, and suggests potential application of the norditerpenoids as novel anti-inflammatory agents for inflammatory disease treatment.

Supplementary Information

The online version contains supplementary material available at https://doi.org/10.1007/s13659-025-00548-1.

Additional file 1. The 1D and 2D NMR, HRESIMS, and IR spectra of 1 – 3, and ECD calculations data for 2 and 3.

Acknowledgements

This work was supported by the National Natural Science Foundation of China (Nos. 82273804, 82304322, 82404454, and 22407144), the Science and Technology Program of Guangzhou, China (No. 2024B03J1322), the Science and Technology Planning Project of Guangdong Province, China (No. 2023A1111120025), the Postdoctoral Fellowship Program of CPSF (No. GZC20242113), the China Postdoctoral Science Foundation (No. 2024M753800), and Jiangxi "Double Thousand Plan" (No. JXSQ2023102240).

Author contributions

JKX carried out the experiment of isolation and structural elucidation and the writing—original draft; LMW screened the biological activities; WYW, DH, SQW, and YJZ analysed the results and did validation; FYY and LL did the ECD calculations and visualization; TY, XC, and GHT carried out the methodology and the writing—review and editing. JLH and SY supervised the whole study, designed and checked the whole manuscript. All authors read and approved the final manuscript.

Funding

This work was funded by the National Natural Science Foundation of China (Nos. 82273804, 82304322, 82404454, and 22407144), the Science and Technology Program of Guangzhou, China (No. 2024B03J1322), the Science and Technology Planning Project of Guangdong Province, China (No. 2023A1111120025), the Postdoctoral Fellowship Program of CPSF (No. GZC20242113), the China Postdoctoral Science Foundation (No. 2024M753800), and Jiangxi "Double Thousand Plan" (No. JXSQ2023102240).

Data availability

The experimental data supporting this work are accessible within the article and its Additional file 1.

Declarations

Competing interests

The authors declare no financial or non-financial competing interests pertaining to this work.

Author details

[1]School of Pharmaceutical Sciences, Sun Yat-Sen University, Guangzhou 510006, China. [2]The Laboratory of Effective Substances of Jiangxi Genuine Medicinal Materials, College of Life Sciences, Jiangxi Normal University, Nanchang 330022, China. [3]School of Life Science and Technology, Wuhan Polytechnic University, Wuhan 430023, China.

Received: 15 June 2025 Accepted: 1 September 2025
Published online: 15 September 2025

References

1. Zhan ZJ, Li S, Chu W, Yin S. *Euphorbia* diterpenoids: isolation, structure, bioactivity, biosynthesis, and synthesis (2013–2021). Nat Prod Rep. 2022;39:2132–74.
2. Chen YN, Ding X, Li DM, Lu QY, Liu S, Li YY, et al. Jatrophane diterpenoids from the seeds of *Euphorbia peplus* with potential bioactivities in lysosomal-autophagy pathway. Nat Prod Bioprospect. 2021;11:375–464.
3. Li CL, Ma MH, Liu X, Hu Y, Feng ZG, Zhang RX, et al. Natural diterpenoids in dermatology: multifunctional roles and therapeutic potential for skin diseases. Phytomedicine. 2025. https://doi.org/10.1016/j.phymed.2025.156842.

4. Vasas A, Hohmann J. *Euphorbia* diterpenes: isolation, structure, biological activity, and synthesis (2008–2012). Chem Rev. 2014;114:8579–612.
5. Tan CJ, Li SF, Huang N, Zhang Y, Di YT, Zheng YT, et al. Daphnane diterpenoids from *Trigonostemon lii* and inhibition activities against HIV-1. Nat Prod Bioprospect. 2020;10:37–44.
6. Lin BD, Zhou B, Dong L, Wu Y, Yue JM. Formosins A-F: diterpenoids with anti-microbial activities from *Excoecaria formosana*. Nat Prod Bioprospect. 2016;6:57–61.
7. Gupta AK, Paquet M. Ingenol mebutate: a promising treatment for actinic keratoses and nonmelanoma skin cancers. J Membr Sci. 2013;17:173–9.
8. McKerrall SJ, Jorgensen L, Kuttruff CA, Ungeheuer F, Baran PS. Development of a concise synthesis of (+)-ingenol. J Am Chem Soc. 2014;136:5799–810.
9. Jorgensen L, McKerrall SJ, Kuttruff CA, Ungeheuer F, Felding J, Baran PS. 14-step synthesis of (+)-ingenol from (+)-3-carene. Science. 2013;341:878–82.
10. Zhang J, Liu M, Wu CH, Zhao GY, Chen PQ, Zhou L, et al. Total synthesis of (−)-pepluanol B: conformational control of the eight-membered ring system. Angew Chem Int Ed. 2020;59:3966–70.
11. Jiang HL, Zhang YY, Mao HY, Zhang Y, Cao YX, Yu HY, et al. Strophiofimbrins A and B: two rearranged norditerpenoids with novel tricyclic carbon skeletons from *Strophioblachia fimbricalyx*. J Org Chem. 2023;88:5936–43.
12. Yang CS, Jiang HL, Mao HY, Zhang Y, Zhang YY, Dong XY. Strophioblin, a novel rearranged dinor-diterpenoid from *Strophioblachia fimbricalyx*. Tetrahedron. 2023;135:133331.
13. Qiu X, Huang YX, Yuan J, Zu XD, Zhou YL, Li R, et al. Strophioblachins A−K, structurally intriguing diterpenoids from *Strophioblachia fimbricalyx* with potential anticardiac hypertrophic inhibitory activity. J Nat Prod. 2023;86:1211–21.
14. Wu XW, Wang BB, Qin Y, Huang YX, Zeb MA, Cheng B, et al. Diterpenoids with unexpected 5/6/6-fused ring system and its dimer from Strophioblachia glandulosa. Chin Chem Lett. 2024;29:110584.
15. Huang JL, Yan XL, Li W, Fan RZ, Li S, Chen JH, et al. Discovery of highly potent daphnane diterpenoids uncovers importin-β1 as a druggable vulnerability in castration-resistant prostate cancer. J Am Chem Soc. 2022;144:17522–32.
16. Gan L, Jiang QW, Huang D, Wu XJ, Zhu XY, Wang L, et al. A natural small molecule alleviates liver fibrosis by targeting apolipoprotein L2. Nat Chem Biol. 2025;21:80–90.
17. Wei X, Huang JL, Gao HH, Yuan FY, Tang GH, Yin S. New halimane and clerodane diterpenoids from *Croton cnidophyllus*. Nat Prod Bioprospect. 2023;13:21.
18. Wu WY, Wei X, Liao Q, Fu YF, Wu LM, Li L, et al. Structurally diverse polyketides and alkaloids produced by a plant-derived fungus *Penicillium canescens* L1. Nat Prod Bioprospect. 2025;15:22.
19. Davison J, Aal F, Cai MH, Song ZS, Yehia SY, Lazarus CM, et al. Genetic, molecular, and biochemical basis of fungal tropolone biosynthesis. PNAS. 2012;109:7642–7.
20. Rudolf JD, Chang CY. Terpene synthases in disguise: enzymology, structure, and opportunities of non-canonical terpene synthases. Nat Prod Rep. 2020;37:425–63.
21. Tang MC, Shen C, Deng ZX, Ohashi M, Tang Y. Combinatorial biosynthesis of terpenoids through mixing-and-matching sesquiterpene cyclase and cytochrome P450 pairs. Org Lett. 2022;24:4783–7.
22. Huang JL, Fan RZ, Zou YH, Zhang L, Yin S, Tang GH. Salviplenoid A from *Salvia plebeia* attenuates acute lung inflammation via modulating NF-κB and Nrf2 signaling pathways. Phytother Res. 2020;35:1559–71.
23. Zou YH, Zhao L, Xu YK, Bao JM, Liu X, Zhang JS, et al. Anti-inflammatory sesquiterpenoids from the traditional Chinese medicine *Salvia plebeia*: regulates pro-inflammatory mediators through inhibition of NF-κB and Erk1/2 signaling pathways in LPS-induced raw264.7 cells. J Ethnopharmacol. 2018;210:95–106.
24. Gantke T, Sriskantharajah S, Sadowski M, Ley SC. IκB kinase regulation of the TPL-2/ERK MAPK pathway. Immunol Rev. 2012;246:168–82.
25. Lu QR, Li L, Cui QY, Liao Q, Malik N, Wu LM, et al. Sclerotiorin-type azaphilones isolated from a marine-derived fungus Microsphaeropsis arundinis P1B. J Nat Prod. 2025;88:1075–84.

Publisher's Note